Desalination and Water Treatment
www.deswater.com
doi: 10.1080/19443994.2015.1019365

57 (2016) 8343–8357
April

Taylor & Francis
Taylor & Francis Group

Synthesis of adsorption cum photocatalytic nature of polyaniline-ZnO/chitosan composite for removal of textile dyes

K. Pandiselvi, S. Thambidurai*

Department of Industrial Chemistry, School of Chemical Sciences, Alagappa University, Karaikudi 630003, Tamil Nadu, India, Tel./Fax: +91 4565 228836; emails: pandismscic@yahoo.co.in (K. Pandiselvi), sthambi01@yahoo.co.in (S. Thambidurai)

Received 13 June 2014; Accepted 8 February 2015

ABSTRACT

The polyaniline-ZnO/chitosan (PZO/chitosan) nanocomposite synthesized using aniline, $ZnCl_2$ and chitosan through precipitation–oxidation method and the synthesized composite was extensively characterized by Fourier transform infrared spectra, UV–vis spectroscopy, scanning electron microscopy, transmission electron microscopy and X-ray diffraction measurements which indicated that the successful formation of ZO nano-rod present inside the chitosan-polyaniline composite. The adsorption and photocatalytic properties of the prepared samples were evaluated by measuring the decrease in concentration of reactive orange after adsorption in the dark and photocatalytic reaction under UV irradiation, respectively. The influences of initial dye concentration, catalyst amount and pH of the reaction solution on reactive orange decolorization were investigated. It was found that the rate of composite/dye interaction was enhanced with the increased load of composite and retarded with the increase in initial dye concentration and pH. Compared with reactive orange, methylene blue as a target pollutant, the adsorption-photocatalytic activities of the resulting composites under different light sources (dark, sunshade, UV and direct sunlight) were also investigated. Results indicates that the maximum color removal were 96% and 88.5% for reactive orange and methylene blue with the corresponding dye concentration 50 mg L^{-1}, PZO/chitosan amount of 0.3 g L^{-1} and neutral pH in 120 min of sunlight exposure respectively. Based on the results, we conclude that PZO/chitosan nanocomposite having both the advantages of photodegradation–adsorption process in the abatement of various wastewater pollutants.

Keywords: Adsorption; Photocatalysis; Polyaniline-ZnO; Chitosan; Nanocomposite

1. Introduction

In recent decades, the field of environmental chemistry, semiconductor mediated photocatalysis has been widely applied in eliminating the organic contamination of water, and has become one of the most important applied facets of heterogeneous catalysis. Among the semiconductors, zincoxide (ZO) possesses some advantages of high optical transmittance, chemical stability, less expensive and environmentally friendly [1]. As a photocatalyst, it can directly degrade various pollutants effectively in wastewater through simple photocatalytic oxidation and reduction reactions. Compared with traditional methods such as adsorption, filtration and sedimentation, photocatalytic

*Corresponding author.

1944-3994/1944-3986 © 2015 Balaban Desalination Publications. All rights reserved.

degradation can directly eliminate the secondary pollution without further treatment, largely decreasing the process cost [2]. Moreover, nanosized ZO photocatalyst often possess higher surface-to-volume ratio than the bulk ZO, supplying more active sites on the surface through this remarkably increasing the degradation rate of pollutants [3,4]. However, nanosized materials have a trend to aggregate in aqueous solution during preparation and utilization through direct inter-particle interactions of Van der Waals forces. In addition, the difficulty in separating and recovering nanosized composite powders from the treated solution seriously limits their practical applications. In this regard, several studies have revealed that chitosan combined with photocatalyst such as niobium (V) oxide [5], Cu_2O [6], CdS [7], TiO_2 and ZO [8–11] have exhibited multifunctional performances in heterogeneous photocatalysis by enhancing the adsorption–photocatalytic process especially for anionic dyes. Chitosan is a natural cationic biopolymer produced by N-deacetylation of chitin, the next preferable natural polysaccharide after cellulose. It contains a large number of reactive hydroxyl (–OH) and amino ($–NH_2$) groups and exhibit unique adsorption and chelating properties for dyes and metal ions [12–14]. On the other hand, heterogeneous-conducting polymer composites have drawn the attention over the past few years. Polyaniline (PA) is one of these polymers that have attracted considerable attention for the preparation of its composites with inorganic particles to improve photocatalytic and adsorption property. Among these particles are TiO_2, MnO_2 and ZO [15–19]. In our previous work, we have studied the adsorption of anionic reactive dye on polyaniline-ZnO/chitosan (PZO/chitosan) hybrid composite by chemical polymerization method [20]. In this study, PZO/chitosan nanocomposites were described for their application in degrading organic dyes under irradiation with UV light, natural sunlight and sunshade. The influences of organic dye type, light source, dye concentration, photocatalyst amount, initial pH and reusing of photocatalyst on the photocatalytic activity were investigated.

2. Materials and methods

2.1. Materials

Chitosan flake (degree of deacetylation: 90%, Mw = 180 kDa) was purchased from M/s South India Sea Foods, Kochi, Kerala, India. Monomer aniline (Merck) was distilled under reduced pressure and stored in dark below 4°C. All other reagents, including Zinc oxide, ammonium persulphate (APS), Reactive Orange 16 ($C_{20}H_{17}N_3Na_2O_{11}S_3$, C.I. 17757, MW: 617.54, certified pure, λ_{max}: 490 nm), Methylene blue ($C_{16}H_{18}ClN_3S_2$. $3H_2O$, C.I. 52015, MW: 373.9, certified pure, λ_{max}: 664 nm), were supplied by Merck. Fig. 1(b) displays the chemical structure of Reactive Orange 16 and Methylene blue. All reagents were of analytical grade and used without further purification.

2.2. Synthesis of PZO and PZO/chitosan nanocomposites

The PA mention the explanation first time doped Zn^{2+} was synthesized using a chemical oxidation and precipitation method according to reported procedure with some modification [21]. The detailed synthesis procedure as follows: Zinc chloride (1.25 g) and APS (1 g) were dissolved in distilled water (100 ml), and then 1 M HCl solution (50 ml) containing 1.02 g of aniline is added to the above solution under vigorous stirring for 1 h at below 5°C. The green water dispersed material is denoted (PA doped Zn^{2+}). Then separately 0.25 g of chitosan was dissolved in acetic acid (4%) under vigorous stirring for 1 h, in which PA doped Zn^{2+} solution was added in a drop-wise manner. After stirred for 1 h, 2 M NaOH was added slowly into the above solution until get the precipitate which is in blue violet color. This was allowed to settle for 24 h followed by washed four times with distilled water (1,000 ml) until the filtrate became colorless then rinsed with ethanol and dried at 80°C for 12 h. This sample is denoted as PZO/chitosan. Fig. 1(c) shows the possible structure of PZO/chitosan. The preparation of polyaniline-ZnO composite under the same procedure except that chitosan was not added, which is denoted as PZO.

2.3. Characterization

The structural information of the samples is measured by FTIR (Perkin Elmer 2000 Model) with KBr as the reference. The crystal structures of the samples are investigated using XRD (Rigaku diffractor with Cu Kα radiation). The morphology and elemental analysis of the samples are characterized by HRSEM (FEI Quanta FEG 200) with an accelerating voltage of 30 kV and a HRTEM using CM200 model at the accelerating voltage 200 kV. For TEM observation, the powdered sample was dispersed in ethanol using ultrasonic bath, and a small amount of the suspension was dropped on the copper grid and air dried. The optical absorption properties of the samples were investigated by UV–vis spectrophotometer (Shimadzu, UV-2401). The pH measurements were carried out with a digital pH-meter (Fisher Scientific, Elico LI120

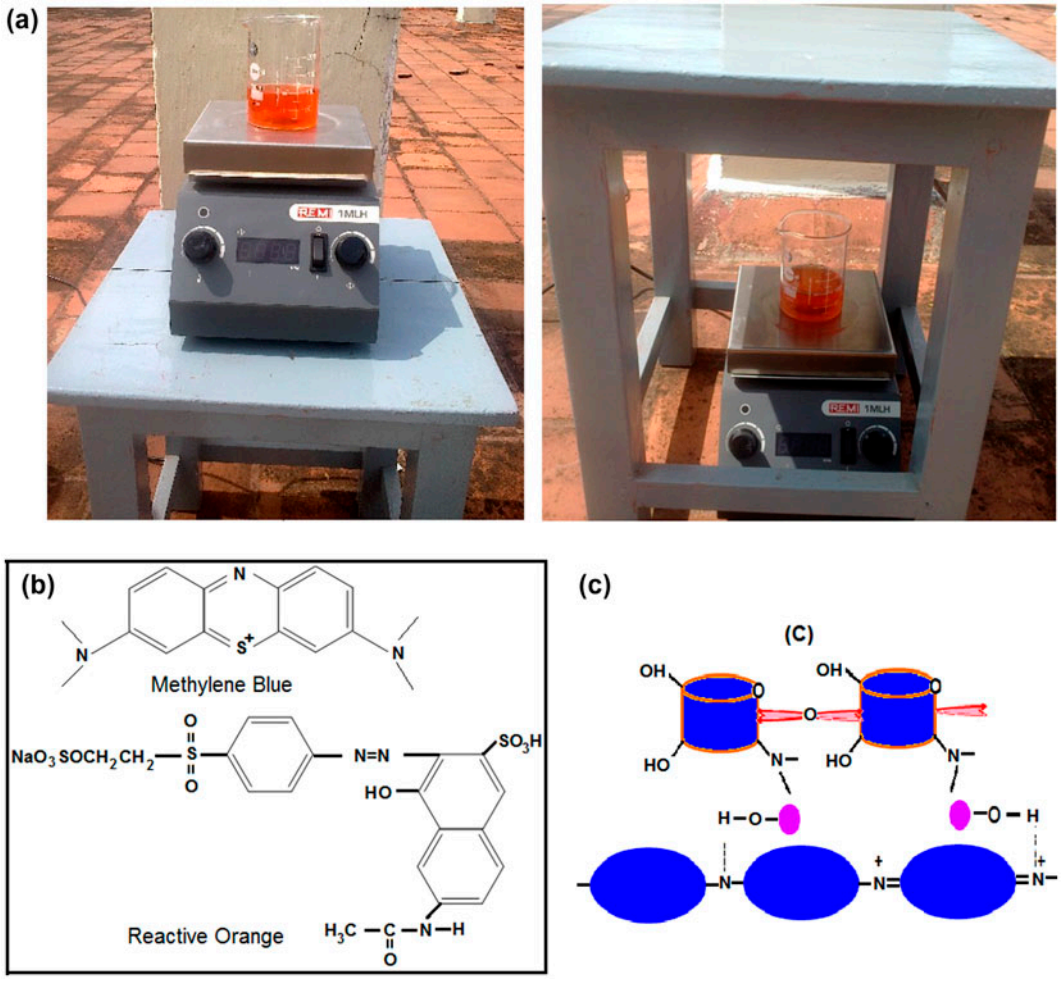

Fig. 1. Schematic representation of (a) decolorization of reactive orange under sunlight/sunshade, (b) chemical structure of methylene blue and reactive orange and (c) possible structure of PZO/chitosan nanocomposite.

model) equipped with a glass electrode. Calibration plots based on Beer–Lambert's law relating to the absorbance of the concentration were established at the maximum absorbance of 494 and 664 nm for reactive orange and methylene blue, respectively.

2.4. Catalytic test

The photocatalytic activities of the synthesized materials were evaluated by photocatalytic decolorization of reactive orange in an aqueous solution under UV light irradiation. A 100 ml of reactive orange solution was mixed with a different catalyst dosage, initial dye concentration and initial pH exposed to the UV-A tube lamp (15 W, length 41 cm, diameter 2.5 cm) model G15T8 (Philips, Holland) was used as the radiation source (λ = 365 nm). The distance between solution and UV source was constant, 14 cm at room temperature, for all experiments. Before irradiation, the suspension was stirred magnetically for 30 min at 100 rpm in dark conditions until adsorption–desorption equilibrium was established. The adsorption capacity, q_e (mg g^{-1}) of dye solutions retained on per gram of adsorbent equilibrium concentration (C_e) was calculated using the equation

$$q_e = \frac{(C_o - C_e)V}{m} \quad (1)$$

where C_o and C_e are the initial and equilibrium concentrations of reactive orange in aqueous solution, V is the solution volume and m is the amount of adsorbent. Followed by this mixture was exposed to the UV light irradiation with stirring to keep the suspension homogeneous and at certain reaction intervals, 5 ml of sample was withdrawn, centrifuged, and the filtrate

transferred into quartz cell to measure the maximum wavelength at 494 nm by UV–vis spectroscopy. The degradation efficiency was calculated as follows:

$$\text{Degradation } \% = \frac{C_o - C_i}{C_o} \times 100\% \quad (2)$$

where C_o (mg L^{-1}) and C_i (mg L^{-1}) are the initial concentration of reactive orange and the concentration at irradiation time t (min), respectively.

2.5. Effect of light sources

The photocatalytic decolorization of reactive orange and methylene blue were carried out under four different light sources like dark, sun shade, UV and sunlight conditions with fixed parameters: dye concentration 50 mg L^{-1}, catalyst concentration: 0.3 g L^{-1}, pH 7.0 and degradation time: 120 min. Dark condition experiments were realized in the dark room to understand the effect of the light source and UV light investigation on solutions using UV-A tube lamb. Sun shade and sunlight reaction were carried out under the shadow and above the table facing direct sunlight (Fig. 1(a)) in the open terrace at 12–2 pm in the month of April to get the uniform light intensity.

3. Results and discussion

3.1. FT-IR spectra

Fourier transform infrared spectrum of chitosan, PA, PZO and PZO/chitosan composites were shown in Fig. 2. Absorption bands of chitosan (Fig. 2(a)) at 1,654, 1,596 and 3,422 cm^{-1} were attributed to its amide I, amide II and hydroxyl functional groups [22,23]. The main characteristic peaks of PA (Fig. 2(b)) are assigned as follows. The band at 3,425 cm^{-1} is attributed to N–H stretching vibration. C=N and C=C stretching modes for quinonoid and benzenoid rings occur at 1,560 and 1,469 cm^{-1}. The bands at 1,298 and 1,236 cm^{-1} are attributed to C–N stretching for benzenoid ring, while the band at 1,101 cm^{-1} can be assigned to quinoid ring of doped PA. The band at 804 cm^{-1} is associated with C–C and C–H for benzenoid ring [24]. After introducing ZO into polyaniline (Fig. 2(c)), the N–H stretching at 3,425 cm^{-1} shifted to 3,439 cm^{-1} indicating the formation of PZO composite [25]. The FTIR spectrum of the PZO/chitosan nanocomposite (Fig. 2(d)) represents the same characteristic peaks with the PZO and broadening of FTIR bands between 2,913 and 3,493 cm^{-1} is due to H-bonding interaction between PA and chitosan [26]. However, the corresponding peaks are shifted to the higher wave numbers, besides their intensities are changed after the addition of chitosan. The peaks of the PZO around 1,558, 1,467, 1,406, 1,297 and 1,126 cm^{-1} are shifted to 1,583, 1,483, 1,410, 1,333 and 1,117 cm^{-1} respectively. This result indicates larger interaction between PZO and chitosan.

3.2. Morphology of PZO and PZO/chitosan

The morphology of PZO and PZO/chitosan characterized by SEM and TEM are shown in Fig. 3. Clearly showed the morphology of PZO (Fig. 3(a)) exhibits irregular spherical particles. No crystalline phase was observed for PZO in the SEM image. Similar result was obtained by Eskizeybek et al. [27]. Fig. 3(b) shows the morphology of PZO/chitosan, from the SEM image of the PZO/chitosan, the mixed shapes of rod, plate and spherical like agglomerated particles, which are different from that of PZO. This observation supports for reason that hexagonal wurzite ZO peaks were clearly displayed in the XRD spectrum of the PZO/chitosan. According to the TEM micrographs in Fig. 3(c), chitosan/PA and ZO nanorods have formed a nanocomposite in which the nanorods are embedded in the polymer matrix with diameters ranging from 20 to 50 nm. In addition the selected area electron diffraction (SAED) pattern is an extremely useful technique that enables to ascertain the structural information of the prepared materials. The SAED pattern of representative PZO/chitosan in (Fig. 3(d)) shows a different planes and the spacing of about 0.281, 0.260 and 0.247 nm which correspond to the planes of (1 0 0), (1 0 2), (1 0 1) hexagonal wurtzite-type ZO crystal [28]. To investigate the chemical composition of the composites, the experiments for the energy-dispersive X-ray spectrum (EDXS) were performed in Fig. 4. From the results of the EDXS, the mass ratio of C, N, O and Zn were calculated in PZO (Fig. 4(a)) is 65.46%:7.66%:14.43%:7.25%. However, the mass ratio of C, N, O and Zn in PZO/chitosan (Fig. 4(b)) is 59.32%:6.46%:12.15%:16.66% respectively. The results clearly indicates that the Zn content is largely increased in PZO/chitosan, comparing with that in PZO, which suggests that these results accorded with SEM and XRD.

3.3. Crystal structure

The XRD patterns of PZO and PZO/chitosan were shown in Fig. 5. For the PZO, the crystalline peaks appeared at $2\theta = 20^\circ$ and 25°, corresponding to parallel

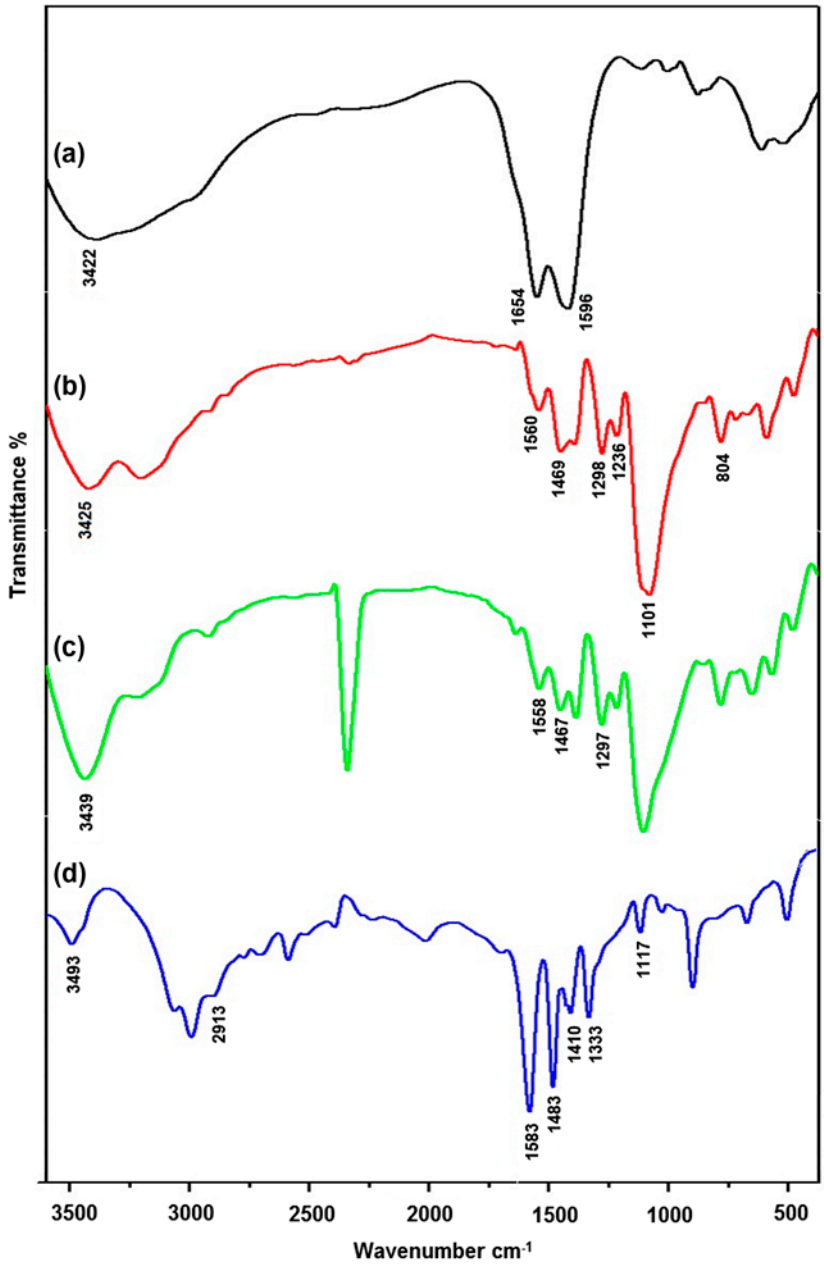

Fig. 2. FTIR spectra of (a) Chitosan, (b) PA, (c) PZO and (d) PZO/chitosan.

and perpendicular to the polymer chain. From this Fig. 5(a), PZO composites showed the peaks which corresponding to PA, revealing that no additional crystalline order had been introduced into the nanocomposites. This indicates that PA deposited on the surface of the ZO and thus the outer layer of the composites is approximately the same as that of pure PA alone [27]. In the pattern of chitosan incorporated PZO, well resembles that of ZO and the diffractive peak of PA has become weak. This result may be attributed that ZO might be deposited on the surface of chitosan/PA composite, which would be very beneficial for photocatalysis of the prepared nanocomposite. Besides, these results indicate that ZO nanoparticles interact with NH_2 and OH groups present in the chitosan/PA moieties. For PZO/chitosan nanocomposite, all the diffraction peaks are well indexed with the JCPDS values (JCPDS No. 30-1451) which shows wurtzite structure of ZO and corresponding to the plane of (1 0 1), (1 0 0), and (1 0 2). The

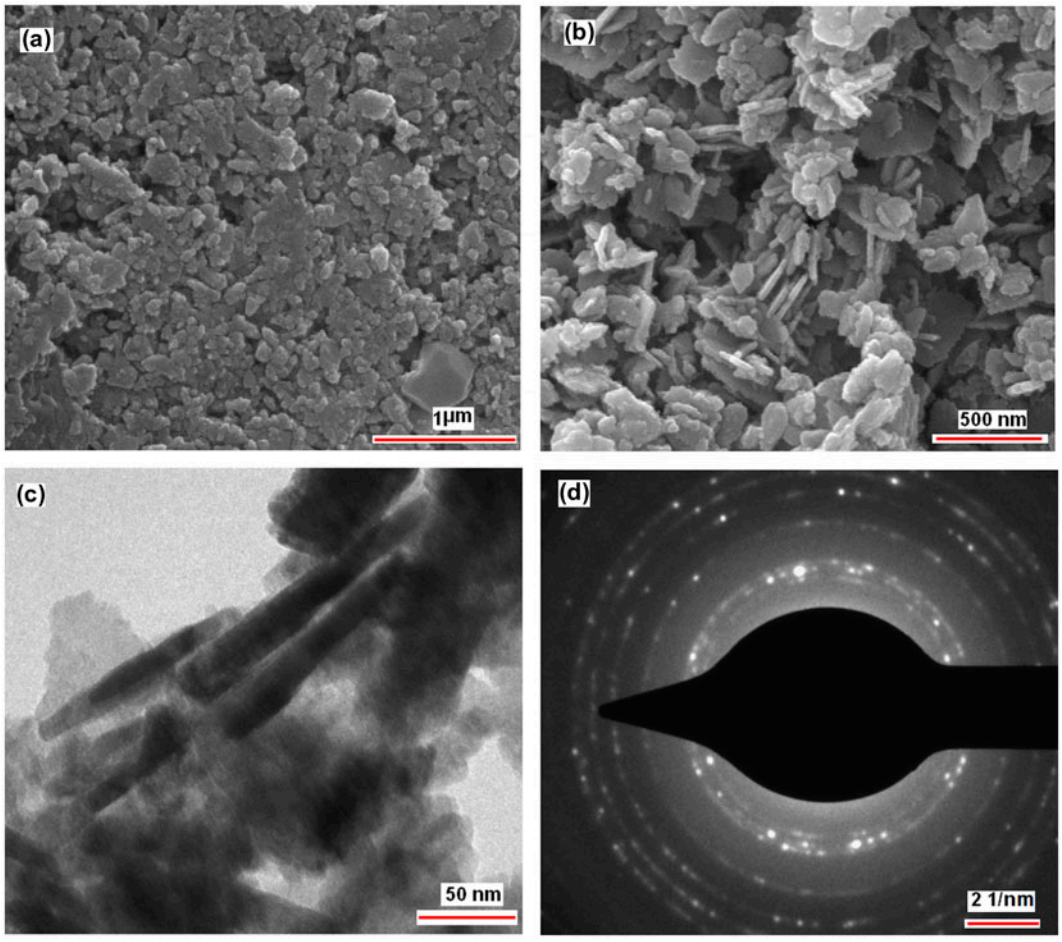

Fig. 3. SEM image of (a) PZO, (b) PZO/chitosan, (c) TEM image of PZO/chitosan and (d) SAED pattern of ZO nanoparticles in PZO/chitosan nanocomposite.

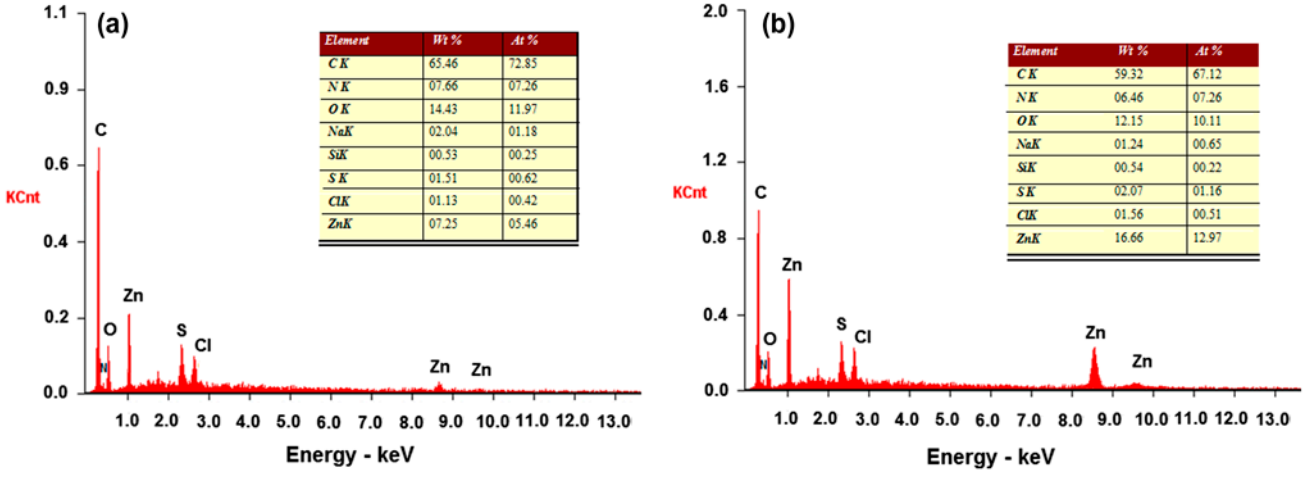

Fig. 4. Elemental analysis for PZO (a) and PZO/chitosan (b) by EDXS.

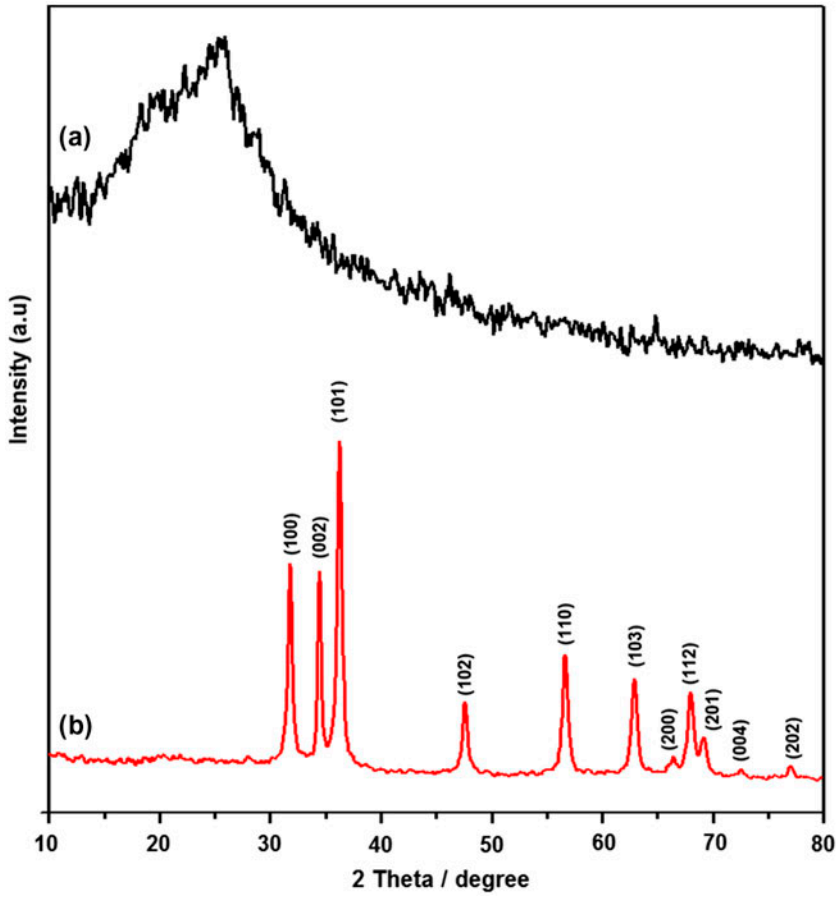

Fig. 5. XRD patterns of (a) PZO and (b) PZO/chitosan nanocomposites.

crystalline size was determined using Debye–Scherrer equation.

$$D = \frac{K\lambda}{\beta \cos\theta} \tag{3}$$

where D is the crystallite size, K is dimensionless constant, λ is the wavelength of X-ray, β is the full width at half-maximum of the diffraction peak and θ is the diffraction angle. Based on the XRD results, it is estimated that the mean size of PZO/chitosan is 30.8 nm, which was accordance with the high magnification TEM image.

3.4. Optical absorption

The optical absorption of the synthesized free PA, PZO and PZO/chitosan composites were measured using UV–vis absorption spectra. As shown in

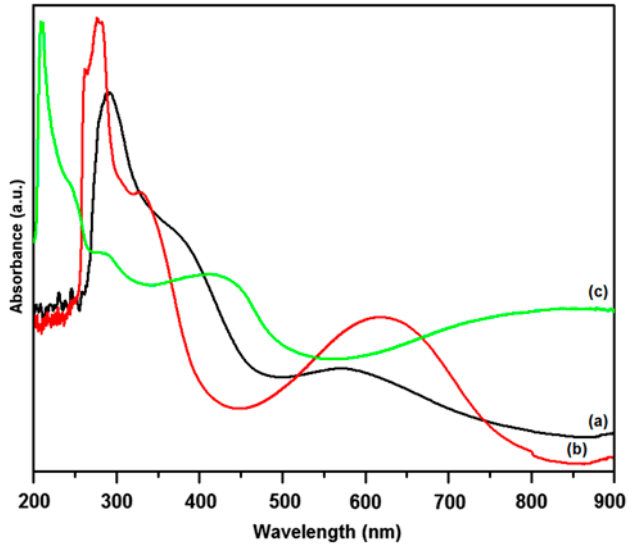

Fig. 6. UV–vis spectra of (a) PA polymer, (b) PZO and (c) PZO/chitosan nano composites.

Fig. 6(a), free PA shows three characteristic absorption peaks around at 290, 392 and 594 nm [29]. The first absorption band arises from π–π* electron transition within benzenoid segments, whereas second and third absorption bands are related to doping level and formation of conducting polarons (quinoid segments), respectively. The PZO composite (Fig. 6(b)) exhibits an absorbance band at 290 nm has shifted to blue and considerable red-shift in band at 594 nm, indicating that the presence of PA on the surface of ZO nanoparticles [30]. The absorption spectrum of the PZO/chitosan nanocomposite was exhibited in Fig. 6(c). In comparison to PZO, the absorption band at 400 and 619 nm that have showed the red shifted and moved to higher wavelength around at 450 and 800 nm, respectively, in PZO/chitosan might due to the successful interaction of PZO and chitosan. Consequently, these effects stated above cooperated to lead to the enhancement of the visible absorption of PZO/chitosan, which was expected to offer an improved photocatalytic activity.

3.5. Adsorption in dark and photocatalysis of reactive orange

To demonstrate the potential applicability, photocatalytic and adsorption experiment were carried out under visible irradiation and in dark respectively. The results are shown in Fig. 7. After 60 min of irradiation time, the decoloriation rates of reactive orange were 34.2, 47.1, 56.12 and 76.1% using ZO, PZO, chitosan-ZO and PZO/chitosan as photocatalyst respectively (Fig. 7(a)), while the decolorization rates were 25.81, 36.97, 50.82 and 64.53% in the presence of ZO, PZO, chitosan-ZO, PZO/chitosan respectively within 60 min in dark, due to the adsorption of dye (Fig. 7(b)). These results implied that the PZO/chitosan exhibited highest adsorption ability and photocatalytic activity, which is ascribed to the synergic effect between chitosan-ZO and PA. The control experiment (photolysis) indicated that no significant decolorization occurred when the dye solution was irradiated with light in the absence of photocatalyst.

3.6. Effect of experimental factors on photocatalytic decolorization of reactive orange

In order to evaluate the photocatalytic performance of PZO/chitosan the effect of key operational factors on photocatalytic decolorization of reactive orange, i.e. catalyst amount, initial dye concentration and solution pH were investigated. The photocatalytic decolorization of dye could be described by pseudo-first-order kinetic Langmuir–Hinshelwood mechanism (Eq. (4)):

$$\ln\frac{C_o}{C_i} = -k_{app}t \tag{4}$$

where k_{app} is the apparent pseudo-first-order reaction rate constant (min^{-1}) and t is the reaction time. A plot of ln (C_o/C_i) vs. t will yield a slope of $-k_{app}$.

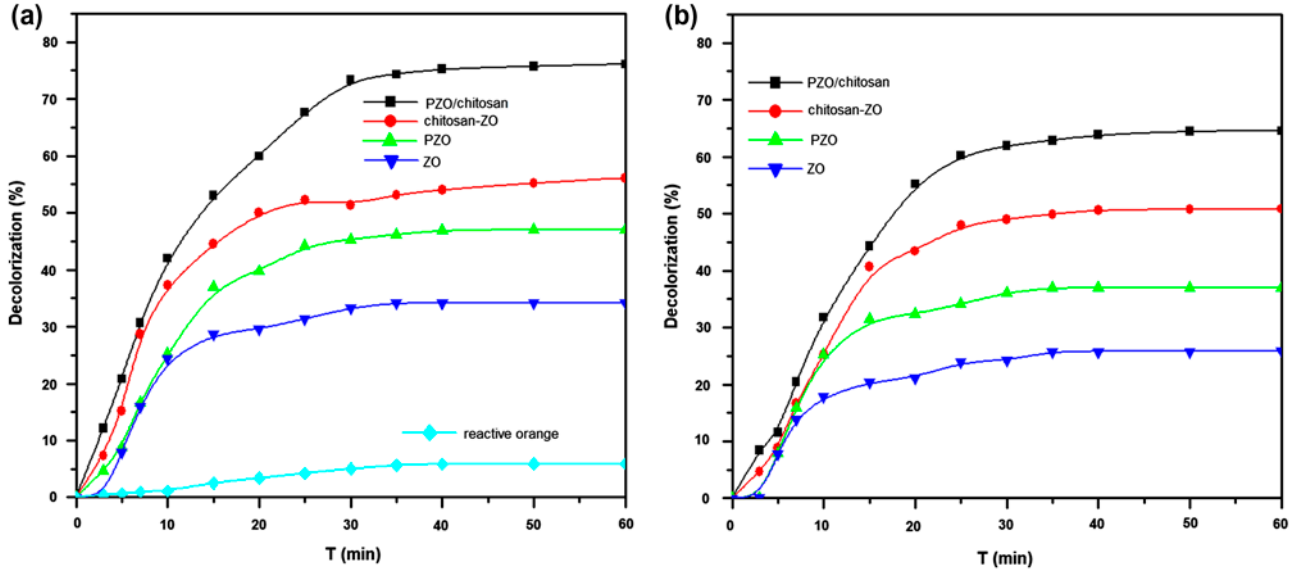

Fig. 7. Decolorization of reactive orange by ZO, PZO, chitosan-ZO and PZO/chitosan samples under (a) dark and (b) UV-light conditions (pH 7.0, dye concentration: 50 mg L^{-1}, catalyst amount of 0.3 g L^{-1}).

3.7. Effect of photocatalyst amount

Effect of catalyst amount on decolorization of reactive orange was studied by varying the dosage of PZO/chitosan nanocomposite from 0.1 to 0.5 g L^{-1}, at a dye concentration 50 mg L^{-1} and pH 7.0. As seen in Fig. 8(a), the decolorization efficiency was directly proportional to the composite mass. A plot of ln (C_o/C_i) vs. irradiation time for different catalyst amounts is shown in Fig. 8(b), the reaction rate constants (k_{app}) for 0.1, 0.2, 0.3, 0.4 and 0.5 g L^{-1} were 0.008, 0.010, 0.014, 0.016 and 0.027 min^{-1}, respectively. This was due to the increase in the number of photons adsorbed and also the number of dye molecules adsorbed with the increase in the catalyst amount [31,32]. For enhancing the decolorization rate and reducing needless waste, 0.3 g L^{-1} was selected as the photocatalyst amount in the experiment.

3.8. Effect of the initial reactive orange concentration

The pollutant concentration is one of important factors for the photocatalytic decolorization efficiency. Fig. 9(a) shows the effect of reactive orange decolorization over the initial concentration range of 25–125 mg L^{-1} under the constant pH 7.0 and catalyst amount 0.3 g L^{-1}. The plot of ln (C_o/C_i) vs. irradiation time for different initial concentration of reactive orange is shown in Fig. 9(b). It is seen that the rate of photocatalytic decolorization is higher when the initial dye concentration is less. The k_{app} values of decolorization reaction were 0.034, 0.029, 0.015, 0.014 and 0.012 min^{-1} at the initial dye concentration of 25, 50, 75, 100 and 125 mg L^{-1} respectively. The reason was that photocatalytic and adsorptive decolorization could be controlled by the limited numbers of reactive sites on the surface of a certain amount of photocatalyst [33]. Another possible reason was that a high initial dye concentration shielded the visible light, which leaded to the reduction in the concentration generated by the hydroxyl radicals [34].

3.9. Effect of pH

The pH plays an important role in the characteristics of dye wastewater and is one of the most important parameters that influence the photo-oxidation processes [35]. The effect of initial solution pH on reactive orange photocatalytic decolorization and the plot of ln (C_o/C_i) vs. irradiation time were performed as and shown in Fig. 10. It was observed that the decolorization rate of reactive orange was higher at lower pH value under constant dye concentration (50 mg L^{-1}) and catalyst amount (0.3 g L^{-1}). The decolorization rates of reactive orange were 99.58, 87.28, 76.21, 67.26 and 62.63%, after 60 min of irradiation, the k_{app} values of dye degradation reaction were 0.033, 0.029, 0.018, 0.011 and 0.008 min^{-1} at pH 3, 5, 7, 9 and 11 respectively. These results indicated that the

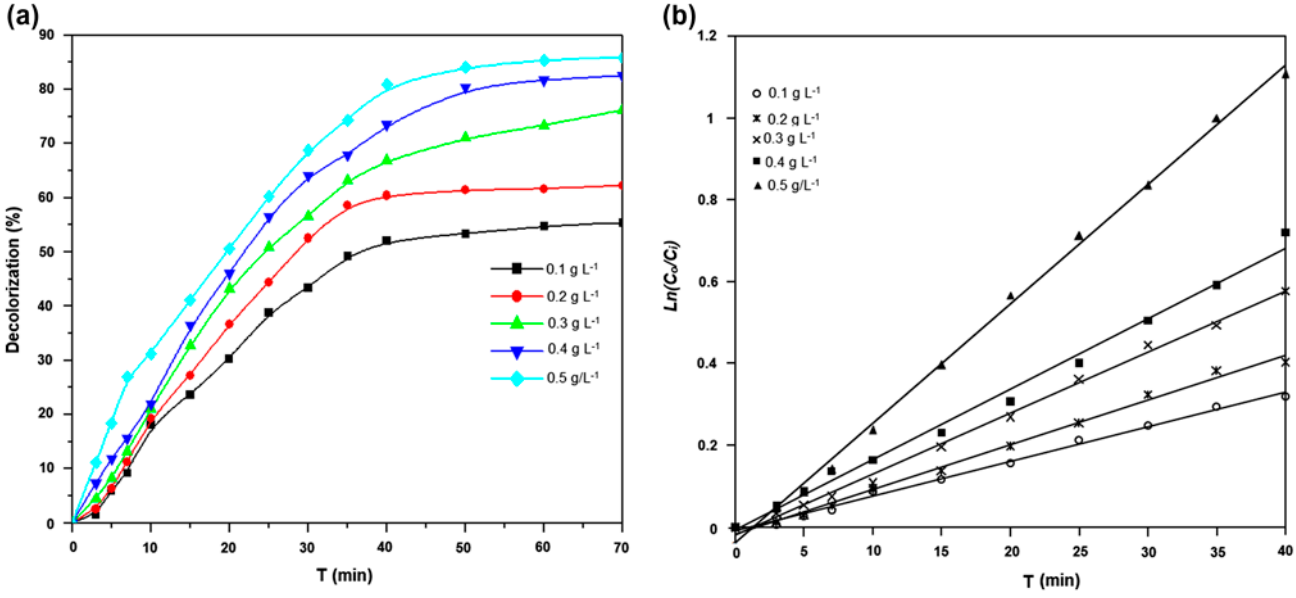

Fig. 8. (a) Effect of catalyst amount on reactive orange decolorization (pH 7.0, dye concentration: 50 mg L^{-1}). (b) Kinetic plot of ln (C_o/C_i vs. T (min), the rate constant k_{app} & R^2 values of 0.1 g L^{-1}: 0.008 min^{-1} & 0.994, 0.2 g L^{-1}: 0.010 min^{-1} & 0.994, 0.3 g L^{-1}: 0.014 min^{-1} & 0.997, 0.4 g L^{-1}: 0.016 min^{-1} & 0.992 and 0.5 g L^{-1}: 0.027 min^{-1} & 0.994.

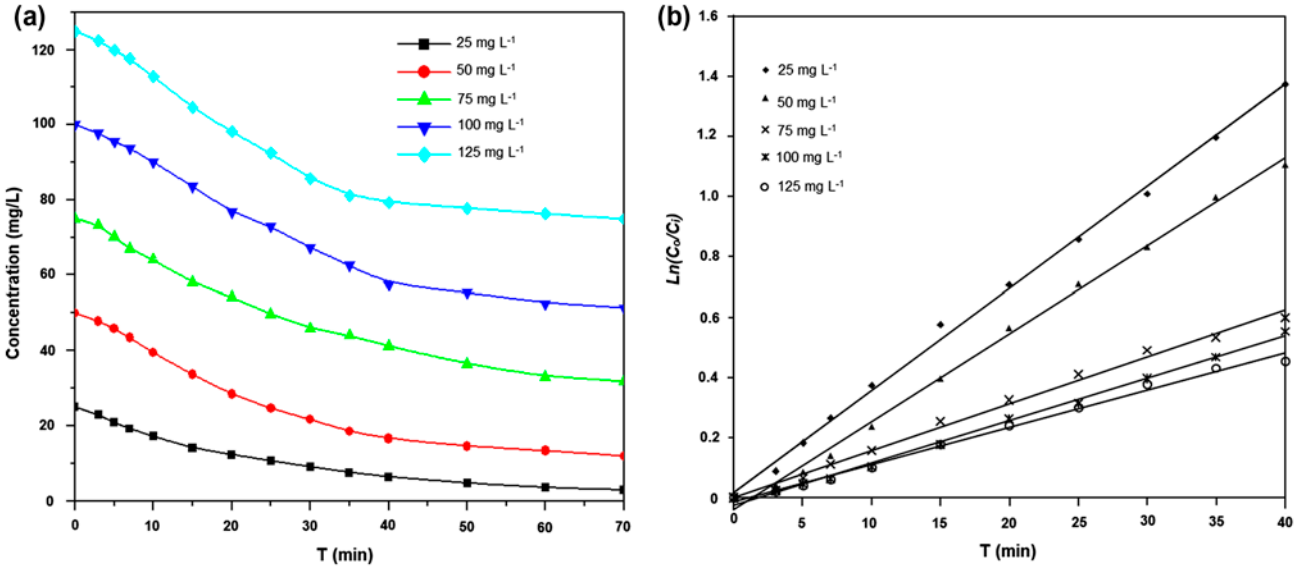

Fig. 9. (a) Effect of initial dye concentration on reactive orange decolonization (pH 7.0, catalyst amount: 0.3 g L^{-1}). (b) Kinetic plot of ln (C_o/C_i) vs. T (min), the rate constant k_{app} & R^2 values of 25 mg L^{-1}: 0.034 min^{-1} & 0.997, 50 mg L^{-1}: 0.029 min^{-1} & 0.997, 75 mg L^{-1}: 0.015 min^{-1} & 0.993, 100 mg L^{-1}: 0.014 min^{-1} & 0.916 and 125 mg L^{-1}: 0.012 min^{-1} & 0.993.

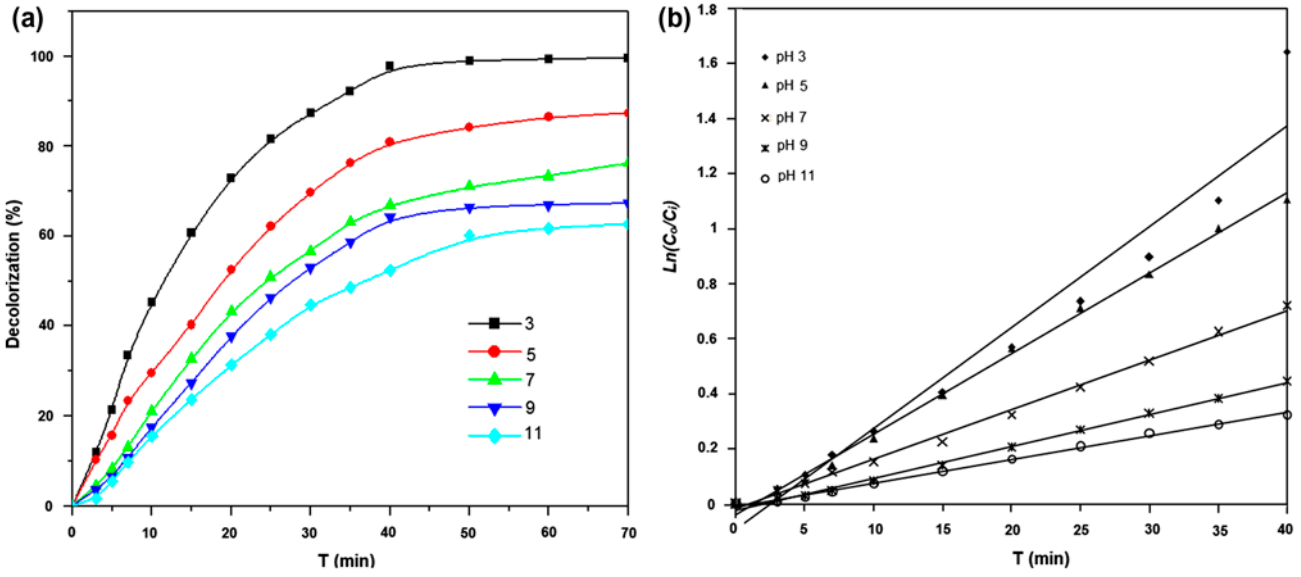

Fig. 10. (a) Effect of initial pH on reactive orange decolorization (dye concentration: 50 mg L^{-1}, catalyst amount: 0.3 g L^{-1}). (b) Kinetic plot of ln (C_o/C_i) vs. T (min), the rate constant k_{app} & R^2 values of pH 3: 0.033 min^{-1} & 0.988, pH 5: 0.029 min^{-1} & 0.996, pH 7: 0.018 min^{-1} & 0.996, pH 9: 0.011 min^{-1} & 0.996 and pH 11: 0.008 min^{-1} & 0.996.

decolorization of reactive orange was more efficient in acidic solution than in basic solution. Since sulfuric groups of dye molecule ionized easily and become a soluble anion, and the residual amino groups of the chitosan/PA on PZO/chitosan surface were more easily to be protonated. Therefore, the reactive orange anions were easily adsorbed to PZO/chitosan nanocomposite with positive surface charge and could be degraded more directly by hydroxyl radicals OH^-) under visible light irradiation in the acidic solution, whereas the neutral and alkaline pHs may deprotonate the emeraldine salt form, transforming the

polymer chains into their emeraldine base (EB) form. If the EB form of polymer is inactive towards the interaction with the dye molecules, then the reaction will be inhibited in alkaline medium. Moreover, the results implied that the adsorption ability significantly influenced the photocatalysis performance of the material. The possible photocatalytic decolorization mechanism of PZO/chitosan nanocomposite in acidic solution may be expressed as follows:

(1) The first step is mainly the adsorption of azo anions on chitosan/PA:

$$R_1 - NH_3^+ + R_2 - SO_3^- \longrightarrow R_1 - NH_3^+ \cdot O_3S - R_2 \quad (5)$$

(1) The second step is photocatalytic decolorization of reactive orange on PZO composite under UV-irradiation, both the PA and ZO absorb photons where the electrons generated by conducting PA can be delivered into the conduction band ZO, enhancing the charge separation and the formation of oxyradicals. The photogenerated holes in the PA species or in ZO particles can migrate to the interface with the solution, which react directly with the surface-sorbed dye molecules or indirectly through the OH radicals to form degradation product.

$$ZnO + hv \longrightarrow ZnO(h^+) + ZnO(e^-) \quad (6)$$

$$ZnO(h^+) + H_2O \longrightarrow ZnO + {}^{\cdot}OH + H^+ \quad (7)$$

$${}^{\cdot}OH + RH \longrightarrow \text{decolorization product} \quad (8)$$

3.10. Comparison of reactive orange and methylene blue decolorization under different light sources

The UV–vis spectra of the original reactive orange and methylene blue dyes and decolorized dyes solutions were kept under four different experimental conditions after 120 min at neutral pH were illustrated in Fig. 11(a)–(d). The maximum absorption region of the reactive orange and methylene blue dyes solution were observed at 490 and 664 nm, respectively. During the sunlight irradiation in the presence of PZO composite (Fig. 11(a) and (c)), the absorbance values at 490 and 664 nm decreased from 1.68 to 0.69 and 3.2 to 1.19. However, the absorbance peaks at the visible region decreased largely after the addition of PZO/chitosan nanocomposite (Fig. 11(b) and (d)) under sunlight irradiation and no displacement of the peak was observed. After these investigations, it is clear that the decolorization efficiency of both reactive orange and methylene blue dyes by the PZO are lower than the PZO/chitosan at all source of irradiation.

Fig. 13(a) and (b) shows the variation in decolorization efficiency of reactive orange and methylene blue verses different light sources in the presence of the PZO and PZO/chitosan composites. In order to investigate the effect of composites/dye interaction, two sets of experiments were carried out. The first set involves the decolorization of reactive orange dye in the presence of the PZO and PZO/chitosan composites under different light sources (Fig. 13(a)). It was observed that the maximum decolorization efficiency of reactive orange in the presence of PZO/chitosan nanocomposite under dark and sunshade conditions, about 83.8 and 84.5%, while UV and direct sunlight irradiation was about 90.1 and 96% (Table 1) respectively. This was because of the anionic functional group of reactive orange dye easily adsorbed with PZO/chitosan composite through electrostatic interaction [36]. In the second set of experiments were conducted under the same conditions using PZO and PZO/chitosan composites by methylene blue under different light sources (Fig. 13(b)). It can be seen that maximum decolorization efficiency of methylene blue under UV and sunlight irradiation, about 43.8 and 88.5% in the presence PZO/chitosan nanocomposite (Table 1). Moreover, the maximum decolorization efficiency of methylene blue dye under UV light irradiation indicates that efficient photocatalytic capability of PZO composite. This result reveals that the PZO/chitosan nanocomposite exhibits the good adsorption performance on reactive orange dye and good photocatalytic performance on methylene blue dye under all source of irradiation. In addition, the electrons transfer from the photocatalytic degradation of the chemisorbed reactive orange dye at the interface of ZO/chitosan to the conduction band of ZO. This adsorption process could also lead to an increase in the dye concentration at the ZO/chitosan interface where a possible charge transfer process could occur at the interface of TiO_2/chitosan since as proven by Janaki et al. [37]. Our studies indicated that, the synthesized PZO/chitosan nanocomposite is more effective on the decolorization of reactive orange and methylene blue dyes under the same conditions to the literature [27] while used 0.3 g L^{-1} photocatalyst and dye concentration 50 mg L^{-1} compare to corresponding

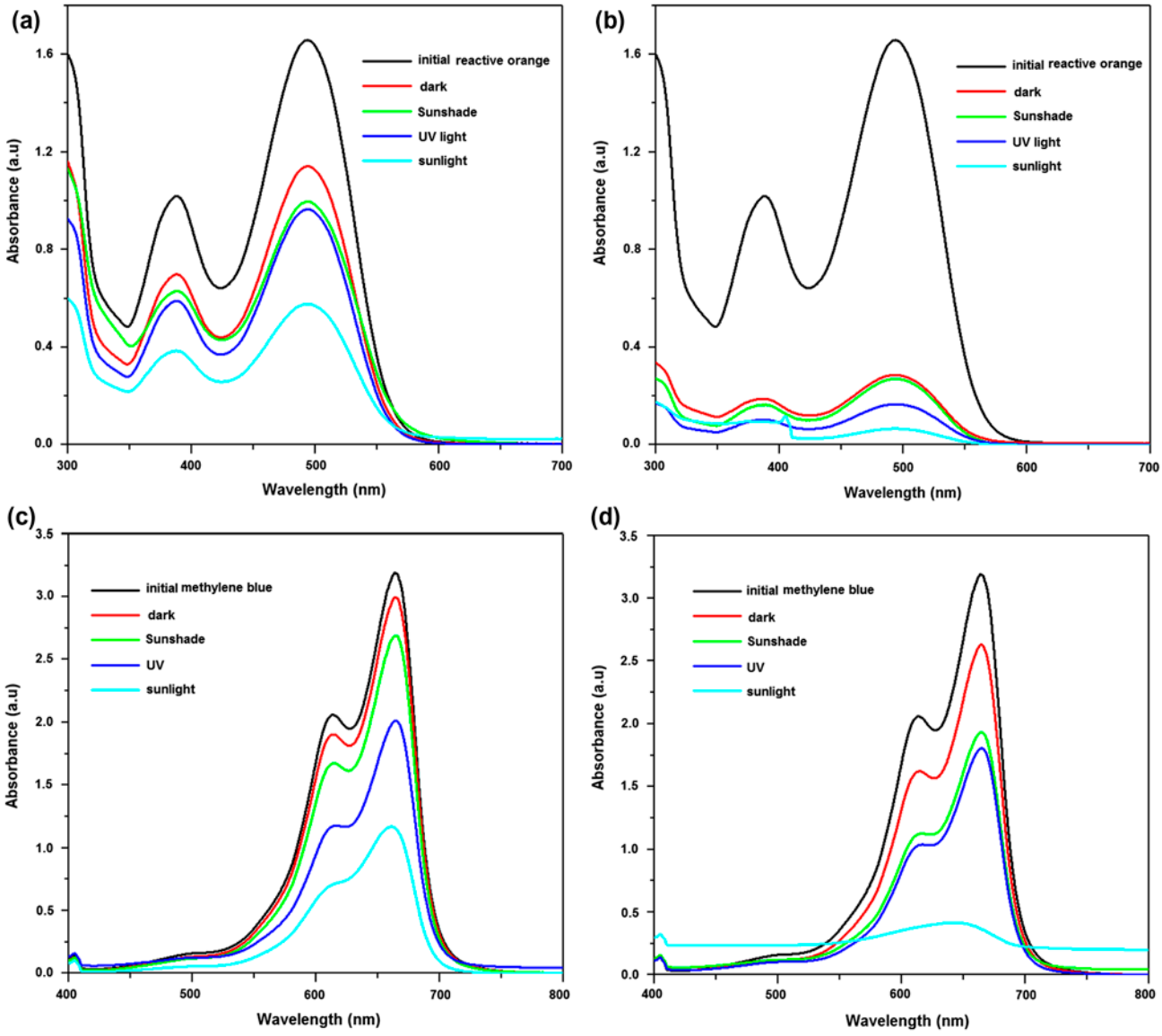

Fig. 11. UV–vis absorption spectra of reactive orange and methylene blue dyes on PZO and PZO/chitosan nanocomposites for different light sources after 2 h. (a) and (b) PZO and PZO/chitosan on reactive orange dye degradation, (c) and (d) PZO and PZO/chitosan on methylene blue dye degradation (catalyst amount: 0.3 g L^{-1}; initial concentration of dye: 50 mg L^{-1} for reactive orange and 25 mg L^{-1} for methylene blue; pH 7.0).

Table 1
Percent removal of reactive orange and methylene blue under different light sources

	Reactive orange			Methylene blue		
Light sources	PZO	PZO/chitosan	Difference	PZO	PZO/chitosan	Difference
Dark	31.1	83.8	52.7	06.2	17.7	11.5
Sun shade	39.9	84.5	44.6	09.5	39.8	30.3
UV light	42.1	90.1	48.0	36.9	43.8	06.9
Sun light	67.5	96.0	28.5	63.8	88.5	24.7

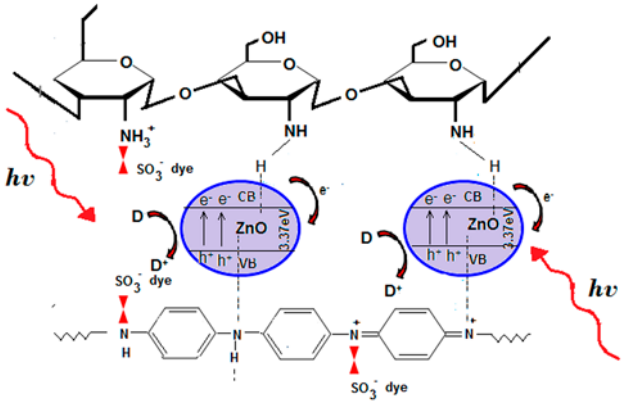

Fig. 12. Possible mechanism involved during adsorption and photocatalytic reaction of dye.

literature for the 120 min sunlight irradiation. In addition, the PZO/chitosan nanocomposite has been compared other types of photocatalysts like PA/TiO_2 and CS/TiO_2 [38,39]. This demonstrates that chitosan would be act as a natural polymer play important role in PZO/chitosan nanocomposite as an effective photocatalyst and also the simultaneous occurrence of the photocatalysis and adsorption process.

The mechanism for adsorption and photocatalysis of PZO/chitosan nanocomposite can be illustrated in Fig. 12, the first step is mainly due to the adsorption of dye anions on chitosan by electrostatic attractions between the SO_3^- groups in reactive orange and the protonated amine groups in chitosan and PA as expressed by Eq. (1). In the second step, presence of UV light irradiation, it is well known that the conduction band electrons (CB^{e^-}) and valence band holes (VB^{h+}) are generated when the PZO composite is irradiated with the UV-light, which energy is greater than either the band gap of PA (2.8 eV) or that of ZO (3.3 eV). The CB^{e^-} react with molecular oxygen to form superoxide radical O_2^{*-}, which ultimately reacts with H^+ to produce HO_2^* radical species. The photo induced holes can react with water and the dye molecule (D) to yield hydroxyl radical and D^{*+} radical cations. All these oxygenous radicals (O_2^{*-}, HO_2^{*-}, OH^{*-}) are powerful oxidizers capable to degrade the organic compound. Further, the reactive D^{*+} radical can transform into oxidation products. When PZO/chitosan nanocomposite is irradiated under natural sunlight, both ZO and PA absorb the photons at their interface, and then charge separation occurs at the interface [27]. As illustrated in Fig. 13, it is believed that the main process that led to the dramatic increase in the rate of decolorization of dyes by the PZO/chitosan after the chitosan sub-layer became saturated was due to a charge transfer process. The process was facilitated by the oxidation of the chemisorbed reactive orange dye is followed by the electron transfer reaction, which plays a vital role in the initiation of the reactions involving the degradation of the organic dyes.

3.11. Recycle of PZO/chitosan photocatalyst

The catalyst's lifetime is an important parameter of the photocatalytic process, due to the fact that a longer period of time leads to a significant cost reduction of the treatment. It is essential to evaluate the stability and reuse of the catalyst for practical implication.

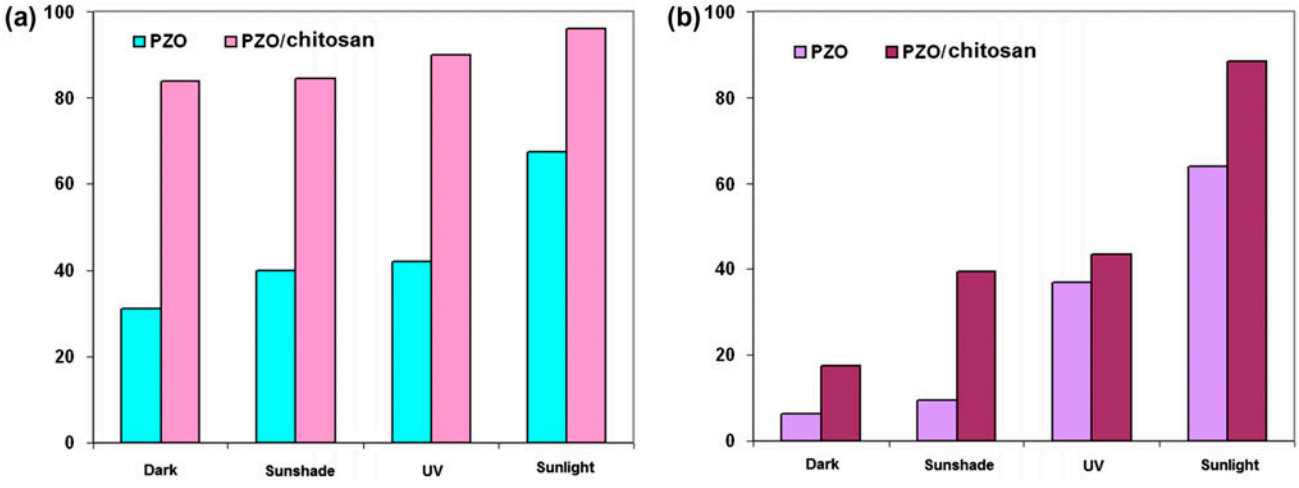

Fig. 13. Decolorization efficiency of (a) reactive orange and (b) methylene blue dyes by PZO and PZO/chitosan nanocomposites under different light sources.

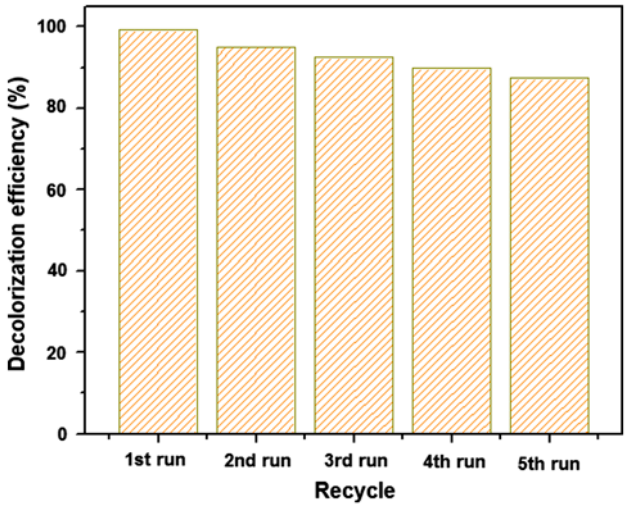

Fig. 14. Stability and recycle of PZO/chitosan (dye concentration: 50 mg L^{-1}, catalyst amount: 0.3 g L^{-1}, pH 3, irradiation time: 60 min).

Fig. 14 shows the repetitive photodegradation of reactive orange during five consecutive cycles with the same 0.3 g L^{-1} catalyst at 50 mg L^{-1} dye concentration, pH 3.0. After each cycle, the PZO/chitosan catalyst was washed with double distilled water and a fresh solution of reactive orange was added before each photocatalytic run. The decolorization rates for the 5 cycling reuse were 99.2, 95.1, 92.5, 89.7 and 87.3%, respectively, after 60 min of irradiation time. It showed a relatively small drop in decolorization efficiency, which was likely due to the loss of the catalyst during washing and filtrating. Thus, the PZO/chitosan photocatalyst is promising for practical application in environment purification.

4. Conclusions

In summary, we have investigated the adsorption and photocatalytic decolorization of reactive orange and methylene blue dyes by PZO composite incorporated with chitosan biopolymer (PZO/chitosan). The results of (FTIR, UV–vis) confirmed that the strong interaction between chitosan, PZO composite and (XRD, TEM) analysis indicated that ZO were embedded in the nanocomposite using chitosan as the induced matrix. Acidic conditions were favorable to promote high adsorption of reactive orange dye onto the chitosan sub-layer, facilitating electron transfer through the oxidized chemisorbed reactive orange to the conduction band of ZO. The maximum decolorization efficiency was achieved by PZO/chitosan nanocomposite under UV and direct sunlight irradiation were significantly influenced by key operational factors, including initial dye concentration (50 mg L^{-1}), catalyst dosage (0.3 g L^{-1}) and initial solution pH (3.0). Thus, the present study reports the PZO/chitosan nanocomposite could be reusable biopolymer, which meant that the adsorption-photocatalytic decolorization process could be operated at a relatively low cost. The results obtained in the study can be useful and helpful in designing an upscalable, practical process for effluent treatment in textile industries under mild conditions.

Acknowledgement

The authors would like to thank the University Grant Commission, New Delhi, India, for providing financial assistance to the first author under Rajiv Gandhi National Fellowship [RGNF No. F. 14-2(SC)/2008 (SC-III) dated March, 2009].

References

[1] Y. Lai, M. Meng, Y. Yu, One-step synthesis, characterizations and mechanistic study of nanosheets-constructed fluffy ZnO and Ag/ZnO spheres used for Rhodamine B photodegradation, Appl. Catal., B 100 (2010) 491–501.
[2] M.J. Height, S.E. Pratsinis, O. Mekasuwandumrong, P. Praserthdam, Ag-ZnO catalysts for UV-photodegradation of methylene blue, Appl. Catal., B 63 (2006) 305–312.
[3] C.J. Murphy, N.R. Jana, Controlling the aspect ratio of inorganic nanorods and nanowires, Adv. Mater. 14 (2002) 80–82.
[4] Q. Wan, T.H. Wang, Enhanced photocatalytic activity of ZnO nanotetrapods, Appl. Phys. Lett. 87 (2005) 083105 (3 pages).
[5] J.D. Torres, E.A. Faria, J.R. SouzaDe, A.G.S. Prado, Preparation of photoactive chitosan-niobium (V) oxide composites for dye degradation, J. Photochem. Photobiol. A 182 (2006) 202–206.
[6] J.Y. Chen, P.J. Zhou, J.L. Li, Y. Wang, Studies on the photocatalytic performance of cuprous oxide/chitosan nanocomposites activated by visible light, Carbohydr. Polym. 72 (2008) 128–132.
[7] H. Zhu, R. Jiang, L. Xiao, Y. Chang, Y. Guan, X. Li, G. Zeng, Photocatalytic decolorization and degradation of Congo Red on innovative crosslinked chitosan/nano-CdS composite catalyst under visible light irradiation, J. Hazard. Mater. 169 (2009) 933–940.
[8] Q. Li, H. Su, T. Tan, Synthesis of ion-imprinted chitosan–TiO_2 adsorbent and its multi-functional performances, Biochem. Eng. J. 38 (2008) 212–218.
[9] Z. Zainal, L.K. Hui, M.Z. Hussein, A.H. Abdullah, I.R. Hamadneh, Characterization of TiO_2–chitosan/glass photocatalyst for the removal of a monoazo dye via photodegradation–adsorption process, J. Hazard. Mater. 164 (2009) 138–145.
[10] C.E. Zubieta, P.V. Messina, C. Luengo, M. Dennehy, O. Pieroni, P.C. Schulz, Reactive dyes remotion by

porous TiO_2–chitosan materials, J. Hazard. Mater. 152 (2008) 765–777.
[11] H.Y. Zhu, L. Xiao, R. Jiang, G.M. Zeng, L. Liu, Efficient decolorization of azo dye solution by visible light-induced photocatalytic process using SnO_2/ZnO heterojunction immobilized in chitosan matrix, Chem. Eng. J. 172 (2011) 746–753.
[12] R. Laus, V.T. de Fávere, Competitive adsorption of Cu(II) and Cd(II) ions by chitosan crosslinked with epichlorohydrin–triphosphate, Bioresour. Technol. 102 (2011) 8769–8776.
[13] M.A. Nawi, S. Sabar, A.H. Jawad, Sheilatina, W.S.W. Ngah, Adsorption of reactive Red 4 by immobilized chitosan on glass plates: Towards the design of immobilized TiO_2 chitosan synergistic photocatalyst-adsorption bilayer system, Biochem. Eng. J. 49 (2010) 317–325.
[14] X.Y. Huang, H.T. Bu, G.B. Jiang, M.H. Zeng, Cross-linked succinyl chitosan as an adsorbent for the removal of Methylene Blue from aqueous solution, Int. J. Biol. Macromol. 49 (2011) 643–651.
[15] H.C. Liang, X.Z. Li, Visible-induced photocatalytic reactivity of polymer-sensitized titania nanotube films, Appl. Catal., B 86 (2009) 8–17.
[16] D.S. Wang, J. Zhang, Q.Z. Luo, X.Y. Li, Y.D. Duan, J. An, Characterization and photocatalytic activity of poly (3-hexylthiophene)-modified TiO_2 for degradation of methyl orange under visible light, J. Hazard. Mater. 169 (2009) 546–550.
[17] M.A. Salem, A.F. Al-Ghonemiy, A.B. Zaki, Photocatalytic degradation of Allura red and Quinoline yellow with polyaniline/TiO_2 nanocomposite, Appl. Catal., B 91 (2009) 59–66.
[18] S. Ameen, M.S. Akhtar, Y.S. Kim, O. Yang, H. Shin, An effective nanocomposite of polyaniline and ZnO: Preparation, characterizations, and its photocatalytic activity, Colloid Polym. Sci. 289 (2011) 415–421.
[19] M. Chang, X.L. Cao, H. Zeng, L. Zhang, Enhancement of the ultraviolet emission of ZnO nanostructures by polyaniline modification, Chem. Phys. Lett. 446 (2007) 370–373.
[20] K. Pandiselvi, S. Thambidurai, Synthesis of porous chitosan–polyaniline/ZnO hybrid composite and application for removal of reactive orange 16 dye, Colloids Surf., B 108 (2013) 229–238.
[21] J. Li, M. Cui, Y. Lai, Z. Zhang, H. Lu, J. Fang, Y. Liu, Investigation of polyaniline co-doped with Zn^{2+} and H^+ as the electrode material for electrochemical supercapacitors, Synth. Met. 160 (2010) 1228–1233.
[22] W. Tan, A.K. Arof, FT-IR studies on interactions among components in hexanoyl Chitosan-based polymer electrolytes, Spectrochim. Acta, Part A 63 (2006) 677–684.
[23] J. Brugnerotto, J. Lizardi, F.M. Goycoolea, W. Argüelles-Monal, J. Desbrières, M. Rinaudo, An infrared investigation in relation with chitin and chitosan characterization, Polymer 42 (2001) 3569–3580.
[24] W. Zheng, M. Angelopoulos, A.J. Epstein, A.G. MacDiarmid, Experimental evidence for hydrogen bonding in polyaniline: Mechanism of aggregate formation and dependency on oxidation state, Macromolecules 30 (1997) 2953–2955.
[25] P.R. Somani, R. Marimuthu, U.P. Mulik, S.R. Sainkar, D.P. Amalnerkar, High piezoresistivity and its origin in conducting polyaniline/TiO_2 composites, Synth. Met. 106 (1999) 45–52.
[26] R. Khan, M. Dhayal, Chitosan/polyaniline hybrid conducting biopolymer base impedimetric immunosensor to detect Ochratoxin-A, Biosens. Bioelectron. 24 (2009) 1700–1705.
[27] V. Eskizeybek, F. Sarı, H. Gülce, A. Gülce, A. Avcı, Preparation of the new polyaniline/ZnO nanocomposite and its photocatalytic activity for degradation of methylene blue and malachite green dyes under UV and natural sun lights irradiations, Appl. Catal., B 119–120 (2012) 197–206.
[28] M. Hojamberdiev, R.M. Prasad, K. Morita, M.A. Schiavon, R. Riedel, Polymer-derived mesoporous SiOC/ZnO nanocomposite for the purification of water contaminated with organic dyes, Microporous Mesoporous Mater. 151 (2012) 330–338.
[29] C.V. Everaldo, P.C. Wang, A.G. MacDiarmid, A class of material incorporating nano/micro self-assembled hollow spheres obtained by aqueous oxidative polymerization of aniline, Synth. Met. 156 (2006) 357–369.
[30] S. Ameen, M.S. Akhtar, S.G. Ansari, O.-B. Yang, H.S. Shin, Electrophoretically deposited polyaniline/ZnO nanoparticles for p–n heterostructure diodes, Superlattices Microstruct. 46 (2009) 872–880.
[31] J. Sun, X. Wang, J. Sun, R. Sun, S. Sun, L. Qiao, Photocatalytic degradation and kinetics of Orange G using nano-sized Sn(IV)/TiO_2/AC photocatalyst, J. Mol. Catal. A Chem. 260 (2006) 241–246.
[32] S. Kaur, V. Singh, TiO_2 mediated photocatalytic degradation studies of Reactive Red 198 by UV irradiation, J. Hazard. Mater. 141 (2007) 230–236.
[33] S. Erdemoğlu, S.K. Aksu, F. Sayılkan, B. İzgi, M. Asiltürk, H. Sayılkan, F. Frimmel, Ş. Güçer, Photocatalytic degradation of Congo Red by hydrothermally synthesized nanocrystalline TiO_2 and identification of degradation products by LC–MS, J. Hazard. Mater. 155 (2008) 469–476.
[34] C.C. Liu, Y.H. Hsieh, P.F. Lai, C.H. LI, C.L. Kao, Photodegradation treatment of azo dye wastewater by UV/TiO_2 process, Dyes Pigm. 68 (2006) 191–195.
[35] A. Franco, M.C. Neves, M.M.L. Ribeiro Carrott, M.H. Mendonça, M.I. Pereira, O.C. Monteiro, Photocatalytic decolorization of methylene blue in the presence of TiO_2/ZnS nanocomposites, J. Hazard. Mater. 161 (2009) 545–550.
[36] M.A. Nawi, A.H. Jawad, S. Sabar, W.S.W. Ngah, Immobilized bilayer TiO_2/chitosan system for the removal of phenol under irradiation by a 45 watt compact fluorescent lamp, Desalination 280 (2011) 288–296.
[37] V. Janaki, B.T. Oh, K. Shanthi, K.J. Lee, A.K. Ramasamy, S. Kamala-Kannan, Polyaniline/chitosan composite: An eco-friendly polymer for enhanced removal of dyes from aqueous solution, Synth. Met. 162 (2012) 974–980.
[38] M.A. Nawi, S. Sabar, Sheilatina, Photocatalytic decolourisation of Reactive Red 4 dye by an immobilised TiO_2/chitosan layer by layer system, J. Colloid Interface Sci. 372 (2012) 80–87.
[39] G. Liao, S. Chen, X. Quan, Y. Zhang, H. Zhao, Remarkable improvement of visible light photocatalysis with PANI modified core–shell mesoporous TiO_2 microspheres, Appl. Catal., B 102 (2011) 126–131.